A&A 462, 919–926 (2007)
DOI: 10.1051/0004-6361:20065712

Astronomy & Astrophysics

HI-observations of blue compact dwarf galaxies. II.⋆

W. K. Huchtmeier[1], A. Petrosian[2], Gopal-Krishna[3], and D. Kunth[4]

[1] Max-Planck-Institut für Radioastronomie, Auf dem Hügel 69, 53121 Bonn, Germany
e-mail: huchtmeier@mpifr-bonn.mpg.de
[2] Byurakan Astrophysical Observatory and Isaac Newton Institute of Chile, Armenian Branch, Byurakan 378433, Armenia
e-mail: artptrs@yahoo.com
[3] NCRA-TIFR, Pune University Campus, Pune 411 007, India
e-mail: krishna@ncra.tifr.res.in
[4] Institut d'Astrophysique, 75014 Paris, France
e-mail: kunth@iap.fr

Received 29 May 2006 / Accepted 14 October 2006

ABSTRACT

We present new results from HI observations of previously undetected 69 blue compact dwarf galaxies (BCDGs) of which 35 BCDGs have been detected (detection rate 51%). Optical data (e.g., from NED) and other literature search are used to estimate the likelihood of confusion from other galaxies within the Effelsberg beam. We have combined 24 BCDG galaxies from this study and from Paper I (Huchtmeier et al. 2005) that are unlikely to suffer from confusion effects in combination with 19 other similar BCDGs taken from the literature to infer several characteristic properties of the BCDG population. The parameters which were used for the statistical analysis include linear diameter, axial ratio, blue luminosity, HI and total masses, HI and total mass-to-blue luminosity ratios, HI to total mass ratio, HI gas velocity dispersion, oxygen abundance, equivalent width of Hβ emission line and $B-V$ color. The analysis has revealed that: BCDGs with higher HI mass tend to have lower abundances of heavy elements and are more compact; BCDGs with lower blue luminosity have larger equivalent width of Hβ emission line and bluer $B-V$ colors, as well as a tendency towards lower abundances of heavy elements; BCDGs with larger linear size, with higher total mass and those with higher total and HI mass per unit blue luminosity, tend to have broader HI emission line (larger velocity dispersion); there is no obvious dependence of the star formation parameters on the total mass; almost 10% of the BCDGs emit milli-Jansky level radio continuum near 1 GHz.

Key words. galaxies: general – galaxies: dwarf – galaxies: evolution – galaxies: abundances – galaxies: starburst – radio lines: galaxies

1. Introduction

Blue Compact Dwarf Galaxies (BCDGs) represent the subset of low-luminosity galaxies undergoing strong and short-lived episode of star formation at the present time. Starting from the pioneering work of Searle & Sargent (1972), this class of galaxies has attracted increasing attention. However, the origin and peculiar nature of their starbursts is still poorly understood. HI observations of BCDGs are therefore important, for not only do they provide estimate of the total mass, but also reveal their HI content which is the raw material for the star formation. Both these, when combined with parameters like absolute luminosity, oxygen abundance etc., can furnish useful clues. In the first article of this series we presented HI observations of 56 BCDGs with the 100-m Effelsberg radiotelescope (Huchtmeier et al. 2005, hereafter referred to as Paper I). Recently, the full catalogue of the Second Byurakan Sky Survey (SBS) has been published (Stepanian 2005), most of which lack HI observations or detections. In this paper, we present sensitive HI observations of a sample of 69 BCDGs assembled from the SBS catalogue for which HI observations (or detection) has not been reported in the literature. Details of the sample are given in Sect. 2. The following sections present the HI observations, the deduced HI parameters, and a discussion of the results which also makes use of the data presented in Paper I, as well as the variety of optical observations gathered from literature, including the Sloan Digital Sky Survey (SDSS), and NED.

2. The sample of BCDGs

The sample of 69 BCDGs was selected from the Second objective prism surveys of active and star forming galaxies, conducted at Byurakan Observatory (Armenia). Detailed information on the Second Byurakan Survey (SBS) (Markarian & Stepanian 1983; and the following papers) can be found in Stepanian (2005) and Petrosian et al. (2006a).

The selection criteria employed for this BCDGs sample are:

- $M_{\rm p}$ fainter than –17-mag, taking $H_0 = 75$ km s^{-1} Mpc^{-1};
- compact structure and a clear absence of spiral arms, or an obvious irregular morphology, as confirmed by high resolution imaging;
- the presence of strong and narrow emission lines;
- no observation (or detection) of the 21 cm HI emission line reported in the literature.

3. H I-observations and basic results

The HI observations were made using the 100-m radiotelescope, which has a half power beam width of 9.3′ at a wavelength of 21 cm. The 1024-channel autocorrelator was split

⋆ Figure 1 is only available in electronic form at http://www.aanda.org

into four filter banks (256 channels each) using a bandwidth of 6.25 MHz which yielded a resolution of 6 km s^{-1} or 10 km s^{-1} after Hanning smoothing. A typical observing time of 60 min per source yielded a rms noise of ∼4 mJy (the system noise was 30 K). Most of the observations were repeated in order to improve the signal-to-noise ratio and the reliability. An ON-source position was combined with an OFF-source position every 10 min. This total power mode improves the baseline stability of the spectra. Frequent measurements of well known continuum sources were used to control the pointing and calibration of the telescope. Every two to three hours, a well known line source (e.g., dwarf galaxies) was observed as a system check. The *toolbox* software of the MPIfR was used for the data reduction. The observed spectra were corrected for moderately curved baselines only; this should not introduce additional errors in the estimated velocities and flux densities of the lines since the line profiles are quite narrow in all cases.

From the observed 69 BCDGs, 35 have been detected in HI. This detection rate of ∼51% is markedly lower than ∼79% found for our BCDG sample reported in Paper I (Huchtmeier et al. 2005). The difference probably owes to the ∼2 times higher average redshift for the present sample (0.0159 ± 0.0104 versus 0.0072 ± 0.0040).

The narrow profiles in Fig. 1 correspond to dwarfish galaxies (i.e., $M^{0,i}_{B,T}$ fainter than –15). In some profiles we have cut out the local HI emission from our galaxy (in fact, the difference of the local emission between the ON and OFF positions – total power mode), as it was much stronger than the extragalactic emission.

Table 1 summarizes the observational data: the galaxy name in Col. 1; coordinates (J2000) in Col. 2, as used for the observations (more precise optical coordinates will be published by Petrosian et al. 2006a); the optical dimensions in arcsec corresponding to the blue surface brightness level at 25 mag arcsec^{-2} (Petrosian et al. 2006b) in Col. 3; the blue apparent magnitude (Stepanian 2005; Petrosian et al. 2006b) in Col. 4; the optical heliocenctric radial velocity (Stepanian 2005; Petrosian et al. 2006b) in Col. 5. The HI data follow, i.e., the measured HI flux (Col. 6), the observed peak flux of the line and its rms error in Col. 7 (for non detections only the rms noise is shown), the heliocentric radial velocity derived from the midpoint of the line at 50% of the peak and its error (Col. 8), and the linewidth at a level of 50% of the line peak and, whenever clearly above the noise, the 20% level (Col. 9; uncertain values are followed by a ":"), and comments (Col. 10) where "c" is for possible confusion and "Int" for interacting galaxy.

The derived global parameters for not confused objects from our sample of galaxies are presented in Table 2, the galaxy name in Col. 1, the optical heliocentric velocity (Table 1, Col. 5) has been reduced to the frame of the cosmic microwave background (using NED) $V_{3\mathrm{Kbgd}}$ (Col. 2). We did not use the more accurate HI velocities because of the possibility of confusion in some cases. The distances in Col. 3 have been derived taking a Hubble constant $H_0 = 72$ km s^{-1} Mpc^{-1} (Freedman et al. 2001). Optical diameters in the D_{25} system (Table 1, Col. 3) have been corrected for absorption and for inclination, where the inclination was derived from the axial ratio assuming an intrinsic axial ratio of 0.2 (e.g. Tully 1985, in view of the uncertainties in these inclinations we did not apply corrections for possible type dependance of the intrinsic axial ratio):

$$\log a_0 = \log\, a + 0.09\, A_b - 0.2\, \log (a/b),$$

where the foreground absorption in the blue A_b is from Schlegel et al. (1998, as given in the NED).

The linear diameter $A_{0,i}$ [kpc] follows in Col. 4, the absolute magnitude $M^{0,i}_{b,t}$ corrected for Galactic extinction (Schlegel et al. 1998) and internal absorption in Col. 5. The internal absorption in a galaxy in the B-band, A_i, depends on inclination and luminosity (Giovanelli et al. 1994; Tully et al. 1998; Verheijen 2001; Karachentsev et al. 1999):

$A_i = [1.6 + 2.8(\log V_m - 2.2)] \times \log (a/b)$; $V_m \geq 42.7$ km s^{-1}

$A_i = 0$ – other

$A_i = 0$ – E, S0, dSph.

Here we use the following definition of V_m:

The HI rotational velocity $V_m = W_{50}/(2\sin i)$ corrected for inclination and turbulent motion (Tully & Fouqué 1985) with isotropic non-circular motion parameter $\sigma_z = 8$ km s^{-1}.

The total H I mass (Col. 6) has been calculated using

$$M_{\mathrm{H1}} = 2.355 \times 10^5\, D^2 \int S_v \mathrm{d}v,$$

where D is the distance in Mpc and $\int S_v \mathrm{d}v$ is the integrated HI-flux in Jy km s^{-1}.

The total mass M_T (Col. 7) has been derived from:

$$M_T = \text{const.}\, D\, a_0 \Delta v^2_{0,i},$$

where D is the distance in Mpc, a_0 the corrected optical diameter in arcmin, const. = 33 110, and $\Delta\, v_{0,i}$ the corrected edge-on linewidths at 50% of the peak flux (e.g. Karachentsev et al. 2004).

The HI mass-to-luminosity ratio M_{HI}/L_B, the mass-to-luminosity ratio M_T/L_B, and the relative HI mass M_{HI}/M_T follow in Cols. 8 to 10, respectively.

The radio continuum parameters of the detected BCDGs are based on the NVSS[2] and/or the FIRST[3] surveys at 1.4 GHz (Sect. 4).

4. Comments on individual galaxies

The 21 cm receiver was tuned to the frequency corresponding to the optical radial velocity of each galaxy, hence the HI profile should appear in the center of its frame in Fig. 1. Profiles not centered to their frame might indicate confusion or blending with HI emission from other galaxies within the radio beam.

Around the position of each galaxy in our sample, we examinated a region of 9.3 arcmin radius (i.e. twice the half-power beam width of the Effelsberg telescope) using the Digital Sky Survey (DSS), as well as the velocity and other data provided in the NED. Based on this, if we failed to identify one or more likely sources of confusion to the observed HI profile, we accepted the HI profile to be genuinely associated with the BCDG.

SBS 0743+591B – the wide double-horned HI profile (v = 6485 km s^{-1}) is typical for a spiral galaxy and probably due to UGC 04020 (v_{opt} = 6295 km s^{-1}) at 1.5′ E, confused.

SBS 0926+606 B – confused by SBS 0926+606A (1.5 arcmin south, optical velocity v = 4002 km s^{-1}). The higher velocity peak of the HI profile agrees in velocity with galaxy B (v = 4090 km s^{-1}) and the low velocity extension matches with galaxy A (see Pustilnik et al. 2002).

SBS 1011+575 – in possible confusion with SDSS J101419.34+571348.6 (v = 2970 km s^{-1}), 4′ S, 11s W. The relatively wide observed profile might be due to contribution from this galaxy.

[2] NRAO VLA Sky Survey at 20 cm, Condon et al. (1998).

[3] Faint Images of the Radio Sky at 20 cm, Becker et al. (1995).

Table 1. Observational data.

Galaxy name	RA, Dec (2000) h m s ° [arcmin] [arcsec]	Optical size [arcsec]	m_B	Opt. vel. [km s^{-1}]	HI-flux [Jy]. [km s^{-1}]	HI-Peak flux [mJy]	HI velocity [km s^{-1}]	HI linewidth [km s^{-1}]	Comments
SBS 0743+591B	07 47 46.0 +59 00 27	9.2 × 9.2	18.5	6340	12.3	68 ± 4	6485 ± 2	363 385	c
SBS 0749+582	07 53 50.7 +58 09 11	9.2 × 7.2	19.0	9415		±2			
SBS 0753+581	07 57 22.4 +58 02 15	20.4 × 17.3	17.5	5683		±2			
SBS 0907+593	09 11 06.2 +59 05 53	19.2 × 8.2	19.0	8894		±4			
SBS 0926+606B	09 30 09.4 +60 28 02	42.8 × 16.3	18.2	4122	2.9	28 ± 3	4076 ± 15	101 183	c, Int
SBS 0935+495	09 38 24.0 +49 18 16	12.2 × 9.2	18.5	9249		±2			
SBS 0935+536	09 38 27.0 +53 28 05	18.4 × 16.4	18.0	7140		±3			
SBS 0943+561	09 46 46.6 +55 57 05	13.3 × 10.2	19.0	8850		±2			
SBS 1000+560	10 04 17.9 +55 51 31	25.5 × 22.4	18.5	7500		±3			
SBS 1011+575	10 14 30.3 +57 17 50	21.4 × 17.5	17.5	2918	1.4	17 ± 3	2948 ± 5	92 145	c
SBS 1033+531	10 36 36.4 +52 51 01	31.6 × 17.4	17.0	986	1.0	20 ± 3	551 ± 5	50 60	
SBS 1050+573	10 53 52.2 +57 07 30	10.2 × 7.1	18.5	2005	15.5	101 ± 5	1910 ± 2	212 233	c
SBS 1054+595	10 57 21.3 +59 19 34	15.3 × 9.2	18.5	8363		±5			
SBS 1115+585	11 18 17.3 +58 18 23	43.9 × 29.4	17.5	2007	2.8	42 ± 4	1756 ± 3	91 112	c
SBS 1115+597	11 18 47.4 +59 26 01	22.4 × 13.2	18.0	1585		±3			
SBS 1116+583B	11 19 24.7 +58 03 50	13.3 × 7.2	19.5	9745		±2			
SBS 1118+587	11 21 35.6 +58 29 28	16.3 × 13.2	18.5	8493		±3			
SBS 1122+575	11 25 02.8 +57 16 08	17.3 × 14.2	17.5	2062		±3			
SBS 1128+573	11 31 16.5 +57 04 00	15.3 × 11.2	18.5	1787	0.6	12 ± 3	1665 ± 11	44	
SBS 1133+597	11 36 34.3 +59 25 37	20.4 × 14.3	17.5	3132		±3			
SBS 1136+607	11 39 11.5 +60 30 45	20.4 × 13.3	18.0	3481	7.4	41 ± 3	3481 ± 7	275 299	c
SBS 1137+588	11 49 16.6 +58 36 20	18.4 × 10.3	18.5	2340	0.9	4 ± 2	1958 ± 11	34	c
				2340	0.3	4 ± 2	2469 ± 21	200:	
SBS 1141+576	11 44 16.6 +57 24 32	10.2 × 8.2	19.0	9294		±3			
SBS 1143+588	11 45 58.7 +58 32 06	32.6 × 25.4	15.5	1415	1.6	19 ± 3	1375 ± 8	81	c
SBS 1145+601	11 47 45.1 +59 53 12	40.8 × 38.8	15.3	1233	1.5	20 ± 3	1279 ± 7	80 120	
SBS 1149+596B	11 52 34.0 +59 22 56	5.1 × 3.1	18.0	3351		±4			
SBS 1149+593	11 52 35.6 +59 04 59	21.4 × 20.3	18.0	3243	0.5	6 ± 3	3715 ± 20	135	c
SBS 1159+516A	12 02 04.9 +51 23 40	26.5 × 11.1	18.0	4424		±3			
SBS 1159+545	12 02 02.4 +54 15 51	15.3 × 8.1	18.0	3537		±3			
SBS 1202+606	12 05 16.9 +60 20 20	13.3 × 10.2	18.5	5949		±3			
SBS 1208+531	12 11 00.7 +52 49 57	15.3 × 14.2	16.5	887	1.3	11 ± 3	973 ± 6		
SBS 1210+537A	12 12 55.9 +53 27 38	26.5 × 15.4	16.5	955	0.5	11 ± 2	1154 ± 6	40 56	c
SBS 1210+578	12 13 02.2 +57 32 18	35.7 × 16.4	18.0	5788	2.4	16 ± 4	5755 ± 7	201	
SBS 1211+501	12 13 37.1 +49 50 42	22.4 × 11.2	18.5	6185		±2			
SBS 1212+505	12 14 48.5 +50 16 15	14.3 × 12.3	18.5	4009	0.4	8 ± 2	4029 ± 12	49	
SBS 1212+493	12 14 35.2 +49 06 47	19.4 × 12.2	17.5	3577		±6			
SBS 1215+565	12 17 49.4 +56 14 43	18.4 × 14.3	18.0	4992		±3			
SBS 1216+590	12 18 27.3 +58 45 33	15.3 × 13.3	17.5	4531		±2			
SBS 1216+551	12 19 21.4 +54 51 37	17.4 × 11.3	18.0	5195		±4			
SBS 1219+559	12 21 28.9 +55 38 22	13.3 × 9.1	18.5	9170	1.4	8 ± 2	9101 ±15	400:	
SBS 1219+571	12 21 41.3 +56 49 46	15.3 × 12.2	18.0	4751		±3			
SBS 1221+545B	12 24 23.0 +54 14 48	11.2 × 10.2	18.0	5594		±4			
SBS 1222+588	12 24 51.4 +58 32 41	19.4 × 13.2	17.5	4649		±4			
SBS 1222+614	12 25 05.6 +61 09 10	32.6 × 27.4	17.0	706	2.8	47 ± 3	709 ± 4	65 86	
SBS 1227+563	12 30 07.3 +56 05 14	14.3 × 12.8	19.5	4598	0.5	8 ± 3	4559 ± 12	77	

SBS 1033+531 – the brightest object within the Effelsberg beam. No confusing object in NED. A possible radio counterpart is seen on the NVSS image, with a peak flux of ∼2 mJy at 1.4 GHz. However, non detection in the FIRST survey implies that any emission on arcsecond scale is weaker than 0.5 mJy at 1.4 GHz.

SBS 1050+573 – falls within 1′ of NGC 3440 (v = 1904 km s^{-1}). Radial velocity of the compact dwarf galaxy is swamped by the wide double-horned HI profile due to NGC 3440. An extended radio source of size ∼1.5 × 0.9 arcmin (position angle 58 deg) and flux density of 8.4 ± 1.3 mJy at 1.4 GHz (NVSS), is associated with this BCDG. It is peaked at RA (2000) = 10h 53m 50.5s, Dec (2000) = +57° 07′ 10″. The non detection in the FIRST survey implies that any arcsecond scale component is weaker than 0.5 mJy at 1.4 GHz.

SBS 1115+585 – no HI emission detected at the optical velocity of this BCDG (2007 km s^{-1}), the observed HI-profile is due to UGC 06304 (v = 1762 km s^{-1}).

Table 1. continued.

Galaxy name	RA, Dec (2000) h m s ° [arcmin] [arcsec]	Optical size [arcsec]	m_B	Opt. vel. [km s^{-1}]	HI-flux [Jy]. [km s^{-1}]	HI-Peak flux [mJy]	H I velocity [km s^{-1}]	H I linewidth [km s^{-1}]	Comments
SBS 1228+572	12 31 18.6 +56 57 58	15.3 × 10.2	18.0	4797		±3			
SBS 1248+518	12 50 32.3 +51 34 54	25.5 × 21.4	17.0	3347	0.8	12 ± 3	3309 ± 12	72	
SBS 1249+493	12 51 52.5 +49 03 27	24.5 × 8.1	18.0	7296		±4			
SBS 1307+542	13 09 08.8 +53 56 36	34.7 × 23.6	15.5	2497	6.2	44 ± 4	2510 ± 4	192 212	
SBS 1307+563B	13 09 45.9 +56 02 27	14.3 × 10.1	18.0	4831		±4			
SBS 1309+497	13 11 10.2 +49 31 31	21.4 × 13.3	17.5	2499		±4			
SBS 1319+579A	13 21 22.6 +57 41 29	10.2 × 7.1	18.5	2060	8.4	61 ± 3	2097 ± 3	134 218	c
SBS 1354+597	13 55 39.6 +59 27 40	27.5 × 21.5	17.5	3011		±4			
SBS 1358+554	14 00 32.4 +55 14 46	13.3 × 12.2	17.5	3823	1.6	32 ± 4	3858 ± 7	49 74	c
SBS 1359+504	14 01 14.7 +50 13 23	33.7 × 22.6	16.5	1799	0.6	16 ± 3	1778 ± 5	30	
SBS 1401+502	14 03 00.9 +50 00 42	34.7 × 28.4	16.0	2099	1.7	24 ± 3	1922 ± 5	45 87	
SBS 1403+509	14 05 37.8 +50 42 23	23.5 × 17.4	16.5	1884	1.6	20 ± 4	1895 ± 4	49	
SBS 1410+504	14 12 31.5 +50 14 25	28.6 × 19.4	16.5	1919	2.7	19 ± 4	1876 ± 9	274	
SBS 1420+544	14 22 38.8 +54 14 10	11.2 × 9.2	18.5	6176	1.6	14 ± 3	6377 ± 6	250	c
SBS 1435+516	14 36 45.7 +51 27 36	49.0 × 40.6	15.5	2381	1.8	22 ± 4	2380 ± 6	66	
SBS 1445+543	14 46 40.2 +54 06 45	18.4 × 9.2	17.5	5186		±4			
SBS 1510+571	15 12 12.6 +57 00 08	29.6 × 17.4	16.5	643	0.6	14 ± 3	620 ± 10	43	
					0.7	10 ± 3	822 ± 10	80	
SBS 1533+574B	15 34 14.0 +57 17 04	12.2 × 12.2	16.6	4287	6.6	55 ± 3	3311 ± 3	187	c
SBS 1533+602B	15 34 48.5 +60 05 08	17.3 × 13.2	19.0	2968	0.8	6 ± 2	2834 ± 6	380	c
SBS 1540+576A	15 41 09.5 +57 31 53	27.5 × 14.3	18.0	3717	0.4	8 ± 2	3709 ± 8	88	
SBS 1543+598	15 44 01.6 +59 42 12	13.3 × 10.2	18.5	5156		±3			
SBS 1553+573	15 54 47.6 +57 09 36	33.7 × 27.6	17.0	3610		±3			
SBS 1558+585	15 59 54.6 +58 22 49	23.5 × 17.4	17.5	4218	1.9	17 ± 4	4214 ± 5	133	c
SBS 1614+600B	16 15 41.8 +59 55 37	11.2 × 10.2	18.5	9100		±3			

SBS 1128+573 – the observed HI profile (v = 1665 ± 11 km s^{-1}) is in marginal agreement with the optical velocity (v = 1787 ± 36 km s^{-1}). No obvious confusing object found in NED.

SBS 1133+597 – the FIRST image shows a point-like radio counterpart with flux density of 1.3 ± 0.2 mJy at 1.4 GHz, centered at RA (2000) = 11h 36m 34.9s, Dec (2000) = +59° 25′ 33″.

SBS 1136+607 – the double-horned wide HI profile (v = 3481 km s^{-1}) is typical for a spiral galaxy, probably due to UGC 06619 (v = 3465 km s^{-1}), 3′NE.

SBS 1137+588 – the weak HI emission at v = 2480 km s^{-1}) is in fair agreement with the optical velocity (v = 2340 km s^{-1}). A possible HI feature seen at v = 1958 km s^{-1} could be due SBS 1137+589 (v = 2032 km s^{-1}) 2′E, 2.2′N.

SBS 1143+588 – in possible confusion with the fainter HII galaxy SDSS J114603.39+583621.9 (v = 1414 km s^{-1}) situated 0.6′E and 4.2′N. FIRST map shows a point-like image of 3.6 ± 0.2 mJy at 1.4 GHz.

SBS 1145+601 – the HI velocity (1279 km s^{-1}) is compatible with the optical velocity (1232 km s^{-1}).

A faint radio counterpart is seen on the NVSS image, with a peak flux of 2 ± 0.4 mJy at 1.4 GHz, centred at RA (2000) = 11h 47m 48.3s, Dec (2000) = +59° 53′ 17″. However, non detection in the FIRST survey implies that any arcsecond scale emission is weaker than 0.5 mJy at 1.4 GHz.

SBS 1149+593 – no HI detection at the optical velocity.

SBS 1208+531 – no obvious confusing object in NED. Optical velocity (887 ± 37 km s^{-1}) within the combined errors is compatible with the HI velocity (973 ± 6 km s^{-1}).

SBS1210+537A – velocity of the HI profile (v = 1154 km s^{-1}) does not correspond to the optical velocity (955 km s^{-1} NED). In confusion with SBS 1210+537B at 0.7′ separation.

SBS 1210+578 – the HI velocity (5755 km s^{-1}) is in agreement with the optical velocity (5788 km s^{-1}). This SBS-galaxy is elongated. The broad HI-line is atypical of a dwarf galaxy.

SBS 1212+505 – the HI velocity (4029 km s^{-1}) is in agreement with the optical velocity (4009 km s^{-1}).

SBS 1219+559 – the weak double-peaked profile is too wide for a BCDG object. SBS 1219+559 (v = 9240 km s^{-1}) probably is confused by SBS 1219+558 (v = 9233 km s^{-1}) at 6′. The corresponding HI emisson could be the higher velocity peak. There is no optical counterpart in NED (with matching radial velocity) for the lower velocity HI peak. Due to these uncertainties this galaxy has not been included in Table 2.

SBS 1222+614 – the HI velocity (709 km s^{-1}) agrees well with the optical velocity (706 km s^{-1}).

A faint point-like radio counterpart with ∼1 mJy at 1.4 GHz is seen on the FIRST image.

SBS 1227+563 – the HI velocity (4559 km s^{-1}) is in agreement with the optical velocity (4598 km s^{-1}).

SBS 1248+518 – the HI velocity (3309 km s^{-1}) is in agreement with the optical velocity (3347 km s^{-1}). There is no sign for possible confusion within the radio beam.

SBS 1307+542 – the HI velocity (2510 km s^{-1}) is in agreement with the optical velocity (2458 km s^{-1}) of this galaxy but also of UGC 08231 (v = 2470 km s^{-1}) at 9′ NW. However, situated at 9′ from the SBS galaxy the contribution of UGC 08231 to the observed HI emission would only be of the order of 1 mJy, i.e. less than the noise of the profile.

Table 2. Derived parameters for the detected galaxies

Galaxy name (SBS)	V_{3Kbgd} [km s^{-1}]	Dist. D Mpc	Diam. $A_{0,i}$ kpc	Abs. mag. M_B	HI mass [10^8 $M_\odot$]	Total mass [10^8 $M_\odot$]	M_{HI}/L_B [$M_\odot/L_\odot$]	M_T/L_B [$M_\odot/L_\odot$]	M_{HI}/M_T [$M_\odot/L_\odot$]	Comments
1033+531	1172	16	1.3	–13.60	0.6	2.2	0.9	3.2	0.3	
1128+573	1827	25	4.6	–13.36	0.9	1.9	2.1	4.5	9.5	
1137+588B	2621	36	3.1	–13.98	0.9	56	1.1	64	0.02	
1145+601	1422	20	5.7	–15.78	1.4	83.4	0.3	15.5	0.02	
1208+531	1152	16	2.2	–13.22	0.8	17.9	0.7	16.6	0.04	
1210+578	5908	82	4.0	–16.40	38	206	5.4	29.4	0.2	
1212+505	4221	59	1.8	–15.15	3.2	10.2	1.4	4.4	0.3	
1222+614	838	12	5.3	–12.87	0.9	7.9	2.5	22	0.11	
1227+563	5715	79	5.8	–14.99	7.4	0.9	4.6	5.8	0.8	
1248+518	3482	48	5.9	–16.26	4.4	31.9	0.7	5.3	0.1	
1307+542	2663	37	1.4	–16.97	20	132	1.4	9.0	0.2	
1359+504	1918	27	4.7	–15.40	1.0	1.2	0.3	0.4	0.8	
1401+502	2061	29	3.1	–16.11	3.3	7.7	0.6	1.4	0.4	
1403+509	2030	28	3.1	–15.44	3.0	4.5	0.9	1.3	0.7	
1410+504	2008	28	3.6	–15.36	5.0	160	1.5	49	0.03	N5520
1410+504	2118	29	3.8	–15.36	0.8	3.4	0.22	0.9	0.24	
1435+516	2488	35	8.0	–17.01	5.1	107	0.41	8.7	0.05	
1510+571B	682	9.5	1.2	–13.12	0.13	0.9	0.34	2.5	0.14	
1510+571	884	12	1.6	–13.12	0.25	5.0	0.40	8.0	0.05	U9776
1540+576A	3747	52	6.2	–15.42	2.6	21	0.9	7.6	0.12	

A faint radio counterpart is seen on the NVSS image, with a peak flux of 1.8±0.4 mJy at 1.4 GHz, centred at RA (2000) = 13h 09m 08.6s, Dec (2000) = +53° 56′ 21″. However, non detection in the FIRST survey implies that any arcsecond scale component is weaker than 0.5 mJy at 1.4 GHz.

SBS 1319+579A – this object is the SW compact object projected on an elongated galaxy. SBS 1319+579B is the central condensation of this galaxy. The object "C" is isolated and was not included in the latest SBS catalog (Petrosian et al. 2002). Optical velocities of these three components fall between 1958 and 2060 km s^{-1} and they approach the velocity of the observed HI profile (v = 2096 km s^{-1}). NGC 5109 (v = 2131 km s^{-1}) at 3.8′W, 3′S also matches in the HI velocity. The asymmetric shape of the profile is another hint for confusion.

SBS 1358+554 – in possible confusion with the BCDG SBS 1358+554E at 0.6′. This object is not included in the latest SBS catalog (Stepanian 2005). The HI velocity agrees with the optical velocities of this galaxy pair which is also observed by Comte et al. (1999).

SBS 1359+504 – the velocity of the faint HI emission (1778 km s^{-1}) agrees with the optical velocity (1799 km s^{-1}).

SBS 1401+502 – object is located near the edge of a Schmidt plate, the DSS image covers only part of the field of interest, no obvious confusing objects in NED.

SBS 1403+509 – the optical velocity (1884 km s^{-1}) is in agreement with the HI velocity (1895 km s^{-1}). Only a minor confusion (≤1 mJy) is expected from NGC 5480 (v = 1856 km s^{-1}) 8′ W, due to the strong tapering of the antenna pattern at this distance from the beam center.

SBS1410+504 – the asymmetric HI profile is a hint of confusion. Indeed, the velocity of the HI profile (1876 km s^{-1}) is close to the optical velocity of NGC 5520 (1846 km s^{-1}) at 7′ NW. A secondary peak on the HI profile at v = 1900 km s^{-1} corresponds to the optical velocity (1919 km s^{-1}) of this BCDG. The HI-data in Table 1 correspond to this secondary profile alone.

The NVSS shows a faint radio counterpart, with a peak flux of 1.4 ± 0.4 mJy at 1.4 GHz, centred at RA (2000) = 14h 12m 31.7s, Dec (2000) = +50° 14′ 23″. However, non detection in the FIRST survey implies that any arcsecond scale emission is below 0.5 mJy at 1.4 GHz.

SBS 1420+544 – the velocity of the wide HI profile (6377 km s^{-1}) does not coincide with the optical velocity (6176 km s^{-1}). Moreover, the broad line is not typical for BCDGs. However, there is no obvious sign of a confusing object in NED.

SBS 1435+516 – HI and optical velocities coincide (2380 and 2381 km s^{-1}). NGC 5707 (v = 2212 km s^{-1}) at 9.3′ will not contribute more than 1 or 2 mJy to the observed HI profile.

SBS 1510+571 – the HI profile shows two well separated features (v = 620 and 822 km s^{-1}) which correspond to the optical velocities of this BCDG (v = 643 km s^{-1}) centered to the frame in Fig. 1 and to UGC 09776 (v = 833 km s^{-1}) at 7.7′.

SBS 1533+574B – pairs with the galaxy SBS 1533+574 A. The velocity centroid of the broad HI profile (3311 km s^{-1}) agrees better with the optical velocity of companion A (v = 3348 km s^{-1}) (Petrosian et al. 2002). Possible confusion also with CGCG 297-017 (v = 3282 km s^{-1}) at 5.2′. No HI emission observed at the radial velocity of the galaxy.

A point-like faint radio counterpart (~0.5 mJy at 1.4 GHz) is seen on the FIRST map.

SBS 1533+602B – this broad albeit noisy HI line profile is not typical for BCDGs. Moreover, the optical (v = 2968 km s^{-1}) and HI velocities (2834 km s^{-1}) are only in marginal agreement.

SBS 1540+576A – the radial velocity of the observed narrow HI line (3709 km s^{-1}) agrees well with the optical velocity (3717 km s^{-1}).

SBS 1553+573 – a possible radio counterpart (≤0.5 mJy at 1.4 GHz) is seen near the detection limit of the FIRST survey.

SBS 1558+585 – good agreement between optical (4218 km s^{-1}) and HI velocity (4214 km s^{-1}). A brighter

object, SBS 1559+585 with $v = 4229$ km s^{-1}) at 2.2′ E probably confuses the HI profile (see Paper I).

Thus, from the afore-mentioned discussions, we find that the HI detections in the present sample of 69 BCDGs, 19 BCDGs show no evidence of confusion in their observed HI profiles. Secondly, milli-Jansky level radio emission at 1.4 GHz is found to be associated with the BCDGs SBS 1033+531, SBS 1050+573, SBS 1133+597, SBS 1143+588, SBS 1145+601, SBS 1222+614, SBS 1307+542, SBS 1410+504, SBS 1533+574B and possibly SBS 1553+573 (total 9 BCDGs).

5. Discussion

Mainly during the last two decades, several evolutionary schemes have been developed to unify different morphological classes of dwarf galaxies and to understand their star formation history (e.g. Skillman & Bender 1995; Ferrara & Tolstoy 2000). In all these models, the amount of HI gas is the key ingredient, being the fuel driving the star formation. When HI data are used in conjunction with other parameters of these galaxies, mainly, the metallicity and the stellar population markers, this places constraints on the star formation history (e.g., Lee et al. 2002). Such studies are sensitively dependent on the size of the sample of galaxies and the choice of parameters employed. Combining the HI detected BCDGs from Paper I and the present observations, we count 79 objects for the further statistical study. Out of these total 79 HI detected BCDGs, we have assessed 48 BCDGs to be essentially free from confusion effects (Sect. 4; Paper I). Spectral and photometric information for 24 of these BCDGs could be gathered from the Sloan Digital Sky Survey (SDSS) Data Release 4(DR4) and for a few BCDGs from other literature (Isotov & Thuan 1999; Stepanian et al. 2002; Lee et al. 2004; Petrosian et al. 2006a,b). Further, in order to improve the statistics, we searched the literature to find more BCDGs with published HI, spectral and photometric data, while ensuring that these BCDGs also conform to the defining criteria adopted for our sample (Sect. 2). Our literature search yielded the requisite data for 19 BCDGs, mostly from the articles by Lee et al. (2002, 2004), Salzer et al. (2002, 2005), Thuan & Martin (1981), Petrosian et al. (2006a) and from NED. This brings the total available sample to 43 BCDGs (including 24 BCDGs from our sample, as described above). In all, 12 parameters were selected for statistical study, these are grouped in three categories:

(**a**) integral parameters, namely, linear diameter: $A_{0,i}$ in Kpc; logarithm of axial ratio: $\log b/a$ and logarithm of blue luminosity: $\log L_B$; logarithm of total mass: $\log M_{\rm tot}$ in solar units; logarithm of the total mass to blue luminosity ratio: $\log M_{\rm tot}/L_B$;

(**b**) HI related parameters, namely, logarithm of HI mass: $\log M_{\rm HI}$ in solar units; logarithm of HI mass-to-blue luminosity ratio: $\log M_{\rm HI}/L_B$; logarithm of HI mass-to-total mass ratio: $\log M_{\rm HI}/M_{\rm tot}$ and the HI linewidth at 50% of the peak: W_{50} in km s^{-1}; and

(**c**) parameters related to star formation: oxygen abundance log O/H; equivalent width of Hβ emission line: $EW-$Hβ in Angstroms and $B-V$ color. For the objects with SDSS spectra, oxygen abundances are computed through the direct electron temperature ($T_{\rm e}$) method, or estimated using the ratio [OIII]5007/Hβ, or [NII]6583/Hα, or both emission line ratios (Salzer et al. 2005; Shi et al. 2005). SDSS DR4 ($g-r$) colors were transformed to ($B-V$) colors according to the equation $B-V = 0.62(g-r)+0.15$ of Jester et al. (2005). The number of BCDGs taken from our samples and from the literature, for which we could determine all the 12 parameters, is 43. Table 3 summarizes this information.

We now subject the extensive data available for the 43 BCDGs to the so called, Multivariate Factor Analysis (MFA) (Harman 1967; Afifi & Azen 1979). MFA is a statistical test for detecting correlations among a set of m initial variables measured on n objects, through a reduced number ($p < m$) of linearly independent factors F_1, F_2, ... F_p that presumably account for the correlation. The MFA gives a description, or explanation for the interdependence of a set of variables in terms of the F_i factors without regard to the observed variability. A detailed description of the MFA method can be found in Harman (1967) and Afifi & Azen (1979). This method has been used successfully in astronomy by several authors (e.g., Petrosian & Turatto 1992; Patat et al. 1994; Petrosian et al. 2003). For the present analysis, the parameters in Table 3 have been selected as the initial variables. In order to represent each initial variable with the smaller number of common factors and for a simpler interpretation of the results, we apply the Varimax orthogonal rotation (Kaiser 1958) to the three factors that minimizes the number of common factors for each initial variable. Table 4 shows the factor loadings, i.e. the correlation coefficients between the initial variables and the F_i factors. Accumulated dispersion by the first three Varimax rotated factors is 70%. Adopting $r \sim 0.6$ as correlation threshold, the first rotated factor, F_1, which accounts for about 17% of the common dispersion, is dominated by neutral gas $\log M_{\rm HI}$ and $\log M_{\rm HI}/M_{\rm tot}$ parameters, oxygen abundance (log O/H) and axial ratio (a/b), with higher HI mass BCDGs showing lower abundances of heavy elements and being more compact. This result is in good agreement with Lee et al. (2002). Similar result also was obtained in the HI study of KISS low-luminosity galaxies which are mostly BCDGs, or related objects. Factor two, F_2, describing about 21% of the total variance, correlates optical luminosity of BCDGs with their star formation markers, $EW-$Hβ and $B-V$ color, with lower blue luminosity BCDGs having larger equivalent widths of Hβ emission line and bluer ($B-V$) colors and with a correlation coefficient of 0.472 lower heavy element abundances (log O/H parameter). Similar result for different samples of BCDGs and related low-luminosity galaxies have been obtained in the past (e.g., Salzer et al. 2005; Shi et al. 2005; Lee et al. 2004; Kong et al. 2002; Lee et al. 2006). The third Factor, F_3 (32%), is the combination of the $A_{0,i}$, $\log M_{\rm tot}$, $\log M_{\rm tot}/L_B$, $\log M_{\rm HI}/L_B$ and W_{50} parameters, BCDGs of larger linear size, higher total mass and HI mass per unit blue luminosity, having a larger velocity dispersion of the HI gas. The correlation of HI velocity dispersion with integral parameters has also been noted in some recent studies (e.g. Lee et al. 2002) and the positive correlation between luminosity of BCDGs and their HI gas velocity dispersion is a reflection of the well known Tully-Fisher (1977) relation for this sample of dwarf galaxies. According to the theory underlying the MFA, the factors are orthogonal, hence the corresponding initial variables are independent. It means that for this sample of BCDGs there is no obvious relation between star forming parameters and total mass of these galaxies.

6. Conclusions

We have recorded a 51% detection rate in our Effelsberg 21 cm HI observations of a sample of 69 galaxies. For a statistical study of the properties of BCDGs we selected 12 different parameters which group their integral and HI properties, and parameters related to star formation. These data are available for 24 out

Table 3. Objects and parameters for the statistical analysis.

Galaxy	D_0 [kpc]	$\frac{b}{a}$	log L_B	W_{50}	log $M_{\rm HI}$	log $\frac{M_{\rm HI}}{L_B}$	log M_T	log $\frac{M_T}{L}$	Log $\frac{M_{\rm HI}}{M_T}$	$\frac{\rm O}{\rm H}$	$EW(\rm H_\beta)$	$(B-V)$
Mrk 1416	4.3	0.517	8.31	58	9.00	0.36	8.73	0.43	–0.07	7.86	85.00	0.30
Mrk 1446	6.8	0.879	8.75	50	8.54	–0.21	9.29	0.53	–0.74	8.13	77.10	0.25
Mrk 1450	1.7	0.875	8.27	77	7.30	–0.97	9.08	0.82	–2.00	7.98	123.60	0.14
Mrk 1460	1.2	0.650	7.43	36	6.78	–0.65	7.70	0.28	–0.89	8.11	58.30	0.32
SBS 0943+543	2.2	0.632	7.71	46	7.00	–0.71	8.23	0.53	–1.10	8.28	24.90	0.27
SBS 1006+578A	3.1	0.469	8.07	105	8.45	0.38	9.12	1.04	–0.68	8.28	4.70	0.32
SBS 1054+504	3.0	0.613	8.35	56	7.48	–0.87	8.58	0.23	–1.05	8.23	18.22	0.43
SBS 1114+587	3.1	0.846	8.23	52	7.78	–0.45	8.86	0.62	–1.05	8.24	5.14	0.38
SBS 1118+578B	3.7	0.875	8.51	43	7.78	–0.73	8.85	0.34	–1.10	8.26	5.90	0.40
SBS 1128+573	1.8	0.730	7.54	44	7.95	0.42	8.28	0.65	–0.30	8.17	113.90	0.13
SBS 1205+557	2.3	0.722	7.95	61	7.48	–0.47	8.66	0.76	–1.15	7.91	83.10	0.26
SBS 1208+531	1.2	0.930	7.48	80	7.90	0.42	9.25	1.22	–1.40	8.11	28.30	0.31
SBS 1211+540	1.1	0.813	7.23	47	7.30	0.07	8.23	1.00	–0.85	7.64	124.50	0.11
SBS 1212+505	4.0	0.860	8.25	49	8.51	0.25	9.01	0.64	–0.52	7.95	101.40	0.26
SBS 1222+614	1.8	0.840	7.34	65	7.95	0.61	8.90	1.34	0.96	8.02	87.20	0.15
SBS 1227+563	5.3	0.790	8.19	49	8.87	0.68	8.97	0.76	–0.10	8.03	24.40	0.32
SBS 1248+518	5.8	0.840	8.70	72	8.64	–0.05	9.50	0.72	1.00	8.19	4.70	0.36
SBS 1423+517	4.3	0.613	8.35	79	8.26	–0.10	9.11	0.77	0.85	8.26	131.90	0.31
SBS 1428+457	6.1	0.919	8.87	119	9.01	0.14	10.25	1.39	1.22	8.26	85.10	0.27
SBS 1430+526	7.5	0.829	8.83	72	9.03	0.20	9.57	0.73	–0.54	8.03	42.69	0.27
SBS 1435+516	8.0	0.830	9.00	112	8.71	–0.29	10.03	0.94	1.30	8.40	2.70	0.39
SBS 1453+526	5.6	0.500	8.67	199	8.49	–0.18	10.95	1.25	1.52	8.08	71.28	0.34
SBS 1510+571B	1.6	0.590	7.44	43	7.40	–0.04	8.70	0.90	1.30	8.26	6.00	0.35
SBS 1540+576A	6.2	0.520	8.36	88	8.41	0.05	9.32	0.88	–0.92	8.24	4. 90	0.32
Data from the literature												
Mrk 0067	1.6	0.690	7.80	62	7.42	–0.38	8.86	1.06	–1.44	8.21	82.60	0.09
Mrk 0475	1.2	0.680	7.67	40	8.27	0.60	8.36	0.69	–0.09	7.93	138.90	0.02
Mrk 0487	1.1	0.920	7.96	75	7.45	–0.51	8.87	0.91	–1.42	8.06	164.94	0.24
Mrk 0600	3.0	0.440	8.55	73	8.54	–0.01	9.28	0.73	–0.74	7.83	31.30	0.30
Mrk 0996	3.6	0.760	8.91	83	7.18	–1.73	9.47	0.56	–2.29	7.98	129.00	0.27
Mrk 1308	3.4	1.000	8.91	31	6.65	–2.26	8.59	–0.33	–1.94	8.67	12.00	0.39
IZw18	0.9	0.670	7.72	53	7.84	0.12	8.49	0.77	–0.65	7.18	100.00	–0.06
IIZw40	1.7	0.390	7.76	99	8.38	0.62	9.30	1.54	–0.92	8.09	283.00	0.10
IIZw70	4.3	0.350	8.68	69	8.57	–0.11	9.39	0.71	–0.82	8.06	49.00	0.27
VIIZw403	1.6	0.570	8.03	43	8.25	0.22	8.58	0.55	–0.33	7.69	155.30	0.38
KISSR0096	6.1	0.650	8.92	55	9.25	0.34	9.34	0.42	–0.09	7.91	32.00	0.43
KISSR0133	6.8	0.460	8.99	40	7.96	–1.03	9.11	0.12	–1.15	8.14	8.50	0.54
KISSR0286	3.8	0.890	8.81	211	8.79	–0.02	10.31	1.49	–1.51	8.17	50.00	0.56
KISSR0310	4.5	0.730	8.98	168	8.68	–0.31	10.18	1.20	–1.50	7.88	136.00	0.60
KISSR0396	4.4	0.400	8.19	47	8.05	–0.13	9.06	0.87	–1.00	7.92	48.94	0.34
KISSR0471	19.4	0.349	8.98	191	9.32	0.32	10.92	1.94	1.60	7.49	39.03	0.15
KISSR0666	9.7	0.620	8.54	58	8.61	0.06	9.59	1.04	0.98	7.77	116.40	0.41
KISSR0785	7.3	0.829	8.75	124	9.01	0.25	10.12	1.37	1.11	7.95	22.80	0.43
KISSR1021	2.4	0.750	8.15	110	8.21	0.06	9.53	1.38	1.32	8.49	11.52	0.32

of the non-confused BCDGs reported in the present work and Paper I. These data in combination with those for 19 other similar BCDGs from the literature are used to infer several characteristics of the BCDG population of 43 galaxies. Some statistically significant trends found for our sample are:

1. BCDGs with greater HI mass have lower abundances of heavy elements and are more compact. Such a correlation first given by Chamaraux (1977) is in accord with the idea that gas-rich low luminosity galaxies have converted a smaller fraction of their neutral gas into stars (Staveley-Smith et al. 1992).
2. BCDGs having lower blue luminosity show larger equivalent widths of Hβ emission line and bluer $(B-V)$ colors (albeit, the correlation coefficient is only 0.472 for the case of heavy element abundances).
3. Higher HI velocity dispersion is positively correlated with linear size, total mass, HI mass, as well as the HI mass per unit blue luminosity.

These three properties point to the same underlying fact i.e. that gas-rich low luminosity galaxies tend to be metal-poor systems (e.g. Lequeux et al. 1979; Kinman & Davidson 1981; Skillman et al. 1989). Indeed the metallicity – luminosity relationship found by Richer & McCall (1995) holds in our sample although with a large scatter as we expect in small systems undergoing transient bursts of star formation and hence evolving rapidly with time. To a first approximation metallicity anticorrelates with the gas mass fraction as expected from closed box models (cf. Lequeux et al. 1979; Kinman & Davidson 1981; Pagel 1997) but this can not be the whole explanation (Matteucci & Chiosi 1983). Note that not all dwarf galaxies comply with the correlation

Table 4. Varimax rotated factor matrix.

	$F1$	$F2$	$F3$
$A_{0,i}$	0.450	0.441	0.627
b/a	–0.601	0.073	–0.096
$\log L_B$	0.081	0.752	0.444
W_{50}	–0.098	0.105	0.909
$\log M_{\rm HI}$	0.607	0.323	0.524
$\log M_{\rm HI}/L_B$	0.400	–0.073	0.607
$\log M_{\rm tot}$	0.040	0.351	0.899
$\log M_{\rm tot}/L_B$	0.044	–0.350	0.817
$\log M_{\rm HI}/M_{\rm tot}$	0.738	–0.045	–0.473
12 + log O/H	–0.601	0.472	–0.180
$EW(\rm H\beta)$	0.034	–0.708	0.100
$(B-V)$	–0.176	0.807	0.077
Acc. Variance (%)	17	38	70

between metal abundance and luminosity. Indeed many of them appear overluminous for their abundance (Rönnback & Bergvall 1995; Kunth & Östlin 2000). If the underlying correlation is between mass and metallicity this is expected since most BCDGs have lower M/L ratios (see Kennicutt & Skillman 2001, for a thorough discussion of the problem).

4. No dependence is evident between the total galactic mass and the star formation indicators.
   All these results are consistent with previous results for different samples of low-luminosity dwarf galaxies. In particular no more galaxies with extreme properties such as very low metallicity have been found (Kunth & Östlin 2000).
5. At least 7, but probably 9 (i.e., 13%) BCDGs in the present sample show evidence for milli-Jansky level radio continuum at 1.4 GHz. The radio counterpart of the BCDG 1050+573 is clearly resolved (size ~1.5×0.9 arcmin). If the present BCDG sample is combined with the BCDG sample reported in Paper I, then the mJy level radio continuum is detected in at least 12 of the total 125 BCDGs (i.e., nearly 10%).

Acknowledgements. Based on observations with the 100-m radio telescope of the MPIfR (Max-Planck-Institut für Radioastronomie) at Effelsberg. We have made extensive use of the NASA/IPAC Extragalactic Database (NED, which is operated by the Jet Propulsion Laboratory, Caltech, under contract with the National Aeronautics and Space Administration), and the Digitized Sky Survey (DSS–1) produced at the Space Telescope Science Institute under US Government grant NAG W–2166. G.K. thanks the MPIfR (Germany) and A.P. thanks the IAP (France) for hospitality during a period when part of this work was done. The authors thank an anonymous referee for useful comments.

References

Afifi, A. A., & Azen, S. P. 1979, Statistical Analisis: A Computer Oriented Approach (Chicago: Academic Press)
Becker, R. H., White, R. L., & Delfand D. J. 1995, ApJ, 450, 559 (FIRST)
Chamaraux, P., 1977, A&A, 60, 67
Comte, G., Petrosian, A. R., Ohanian, G. A., & Stepanian, J. A. 1999, Astrophysics, 42, 149
Condon, J. J., Cotton, W. D., Greisen, E. W., et al. 1998, AJ, 115, 1693 (NVSS)
Ferrara, A., & Tolstoy, E. 2000, MNRAS, 313, 291
Freedman, W. L., Madore, B. F., Gibson, B. K., et al. 2001, ApJ, 553, 47
Giovanelli, R., Haynes, M. P., Salzer, J. J., et al. 1994, AJ, 107, 2036
Huchtmeier, W. K., Krishna, G., & Petrosian, A. 2005, A&A, 434, 887 (Paper I)
Hurman, H. H. 1967, Modern Factor Analisis, 2nd Ed. (Chicago: Univ. of Chicago Press)
Isotov, Y. I., & Thuan, T. X. 1999, ApJ, 511, 639
Jester, S., Schnerder, D. P., Richards, G. J., et al. 2005, AJ, 130, 873
Kaiser, H. F. 1958, Psychomet., 23, 187
Karachentsev, I. D., Makarov, D. I., & Huchtmeier, W. K. 1999, A&AS, 139, 97
Karachentsev, I. D., Karachentseva, V. E., Huchtmeier, W. K., & Makarov, D. I., 2004, AJ, 127, 2031 [KKHM]
Kennicutt, R. C., & Skillman, E. D. 2001, AJ, 121, 1461
Kinman, T. D., & Davidson, K. 1981, ApJ, 243, 127
Kong, X., Cheng, F. Z., Weiss, A., & Charlot S. 2002, A&A, 396, 503
Kunth, D., & Östlin, G. 2000, A&ARv, 10, 1
Lee, J. C., Salzer, J. J., Impey, C., Thuan, T. X., & Gronwall, C. 2002, AJ, 124, 3088
Lee, J. C., Salzer, J. J., & Melbourne, J. 2004, ApJ, 616, 752
Lee, H., Skillman, E. D., Cannon, J. M., et al. 2006 [arXiv:astro-ph/0605036]
Lequeux, J., Peimbert, M., Rayo, J.-F., Serrano, A., & Torres-Peimbert, S. 1979, A&A, 80, 155
Markarian, B. E. 1967, Astrophys., 3, 34
Markarian, B. E., & Stepanian, J. A. 1983, Astrophys., 19, 354
Markarian, B. E., Lipovetskii, V. A., Stepanian, J. A., Erastova, L. K., & Shapovalova, A. I. 1989, Soobshch. Spets. Astrofiz. Obs., 62, 5
Matteucci, F., & Chiosi, C. 1983, AAP, 123, 121
Mazzarella, J. M., & Balzano, V. A. 1986, ApJS, 62, 751
Pagel, B. E. J. 1997, Nucleosynthesis and Chemical Evolution of Galaxies (Cambridge: University Press)
Patat, F., Barbon, R., Cappellaro, E., & Turatto, M. 1994, A&A, 282, 731
Petrosian, A., & Turatto, M. 1992, A&A, 261, 433
Petrosian, A., McLean, B., Allen, R. J., et al. 2002, AJ, 123, 2280
Petrosian, A., Allen, R. J., Leitherer, C., et al. 2003, AJ, 125, 86
Petrosian, A. R., Navasardyan, H., Cappellaro, E., et al. M. 2005, AJ, 129, 1369
Petrosian, A. R., McLean, B., Allen R. J., & MacKenty, J. 2006a, ApJS, submitted
Petrosian, A. R., McLean, B., Stepanian, J. A., et al. 2006b, in preparation
Pustilnik, S. A., Martin J.-M., Huchtmeier, W. K., et al. 2002, A&A, 389, 405
Richer, M. G., & McCall, M. L. 1995, ApJ, 445, 642
Rönnback, J., & Bergvall, N. 1995, AAP, 302, 353
Salzer, J. J., Rosenberg, J. L., Weisstein, E. W., Mazzarella, J. M., & Bothun G. D., 2002, AJ, 124, 191
Salzer, J. J., Lee, J. C., Melbourne, J., et al. 2005, ApJ, 624, 661
Schlegel, D. J., Finkbeiner, D. P., & Davies, M. 1998, ApJ, 500, 525
Searle, L., & Sargent, W. 1972, ApJ, 173, 25
Shi, F., Kong, X., Li, C., & Chag, F. Z. 2005, A&A, 437, 849
Skillman, E. D., & Bender R. 1995, Rev. Mex. Astron. Astrofis. Ser. Conf., 3, 25
Skillman, E.D., Kennicutt, R. C., & Hodge, P. W. 1989, ApJ, 347, 875
Staveley-Smith, L., Davies R. D., & Kinman, T. D. 1992, MNRAS, 258, 334
Stepanian, J. 2005, Rev. Mex. Astron. Astrofis., 41, 155
Stepanian, J. A., Chavushian, V. H., Carrasco, L., et al. 2002, AJ, 124, 1283
Thuan, T. X., & Martin, G. E. 1981, ApJ, 247, 823
Tully, R. B. 1985, Nearby Galaxies Catalog (Cambridge: Cambridge University Press)
Tully, R. B., & Fisher J. R., 1977, A&A, 54, 661
Tully, R. B., Pierce, J., Huang, J. S., et al. 1998, AJ, 115, 2264
Verheijen, M. A. W. 2001, ApJ, 563, 694

Online Material

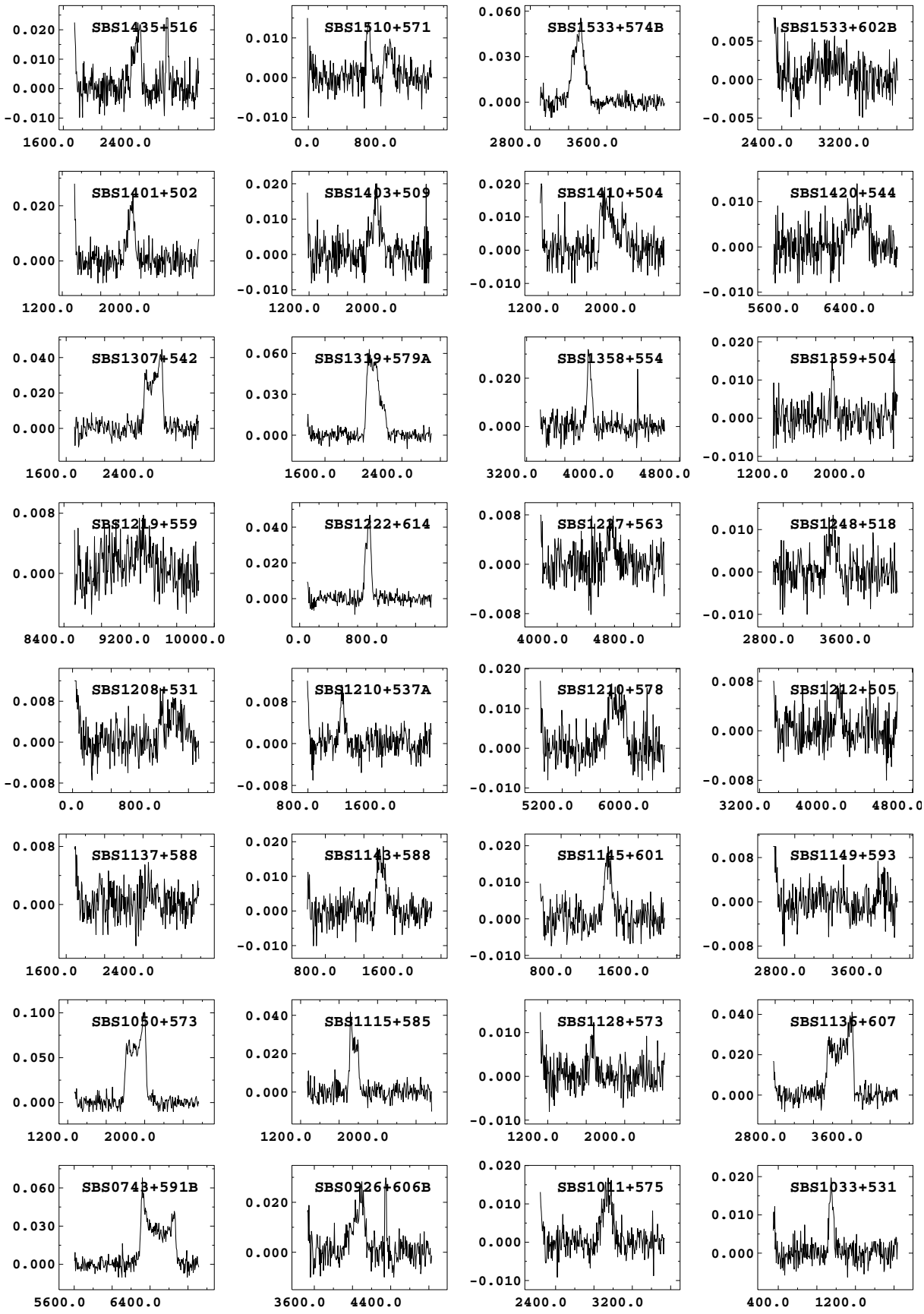

Fig. 1. HI profiles of the 34 BCDGs detected in the present Effelsberg observations, with a pencil beam of half-power beamwidth of 9.3 arcmin at 21 cm. All these galaxies have been detected for the first time. Profiles are arranged in an increasing order of right ascension, starting at the bottom left corner (see Table 1). The axes are labelled in Jansky (Jy) and in heliocentric radial velocity in km s^{-1}. An "X" following the galaxy name indicates possible confusion by another galaxy within the telescope beam (Sect. 4).

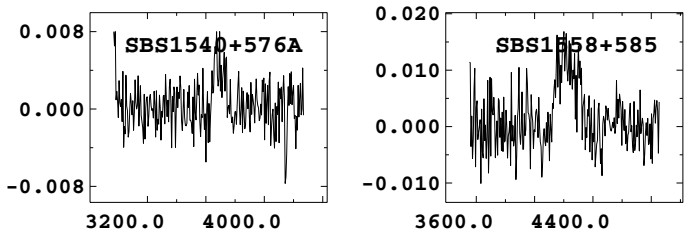

Fig. 1. continued.